CW Autocorrelation Measurements of Picosecond Laser Pulses

KENNETH L. SALA, GERALDINE A. KENNEY-WALLACE, AND GREGORY E. HALL

Abstract—**Completely general and novel expressions are presented for nth-order fast or slow correlation functions, with or without background contributions, from which more specialized nth- and second-order autocorrelation functions are derived. A straightforward method for obtaining CW autocorrelation measurements of picosecond pulses is then described which employs an audio loudspeaker driven at 30 Hz in one arm of the correlator to permit autocorrelation display at this frequency. Results of the application of this device to measurements of the picosecond pulses from a CW synchronously mode-locked Rhodamine 6G dye laser are presented.**

I. Introduction

THE now commonly employed technique of ultrashort laser pulsewidth measurement [1] via autocorrelation in a second-harmonic (SHG) crystal of overlapping "replicas" of a pulse was first reported by Maier, Kaiser, and Giordmaine [2] in 1966 and, immediately thereafter, by Armstrong [3]. The ability of SHG autocorrelation to measure picosecond durations accurately, in essence, stems from the use of accurate, readily controlled increments in length to measure the spatial length of a pulse, and the effectively instantaneous electronic mechanism underlying SHG. The second-harmonic generation autocorrelation technique, however, was largely superceded by the two-photon fluorescence (TPF) method [1], [4] of ultrashort pulsewidth measurement, a principal reason being the fact that, for pulsed lasers, the TPF technique enabled single-shot, single-pulse measurements whereas the SHG technique required several shots while varying path delays in order to produce the complete autocorrelation.

The achievement of CW passive mode locking [1], [5] renewed interest in the SHG autocorrelation technique. With CW mode-locked pulses and the use of a calibrated stepping motor to vary one of the path lengths, it is possible to obtain a pulsewidth measurement easily and accurately in times as short as a few seconds. An important practical advance in this direction is the increase in this "scan" rate to rates $\gtrsim$10 Hz to allow what is best termed a "CW" autocorrelation measurement. Just such an achievement has recently been reported by Fork and Beisser [6] who used a commercial shaker assembly driven at 22 Hz.

Manuscript received March 7, 1980. This work was supported by the Petroleum Research Fund administered by the American Chemical Society, and the National Science and Engineering Research Council of Canada.

K. L. Sala was with the Department of Chemistry, University of Toronto, Toronto, Ont., Canada. He is now with the National Research Council of Canada, Ottawa, Ont., Canada.

G. A. Kenney-Wallace is with the Department of Chemistry, University of Toronto, Toronto, Ont., Canada.

G. E. Hall was with the Department of Chemistry, University of Toronto, Toronto, Ont., Canada. He is now with the Department of Chemistry, Cornell University, Ithaca, NY 14850.

Section II of this paper presents a general, novel treatment of correlation functions which delineates between "fast" and "slow" correlations as well as those with and without background. Section III describes in detail a CW autocorrelator which employs a simple, inexpensive audio speaker to drive one arm of the device and presents measurements made with this device on the picosecond pulses from a CW synchronously mode-locked Rhodamine 6G dye laser.

II. General Expressions for Correlation Functions

Correlation functions can be categorized according to three basic and characteristic properties: correlation functions with background and background-free correlations; "fast" and "slow" correlations; and *cross*-correlation functions as opposed to *auto*correlations. This section presents novel expressions describing in the most general terms possible the nth-order correlation function having an arbitrary trio of the pairs of properties listed above.

A. nth-Order Cross-Correlation Functions

The general nth-order fast correlation function with background for n distinct light pulses having real electric field amplitudes $E_j(t) = \xi(t) \cos [\omega_j t + \phi_j(t)]$ is given by

$$g_B^n(\tau_1, \tau_2, \cdots, \tau_{n-1}) = \frac{\int_{-\infty}^{\infty} \{E_1(t) + E_2(t+\tau_1) + \cdots + E_n(t+\tau_{n-1})\}^{2n} dt}{\int_{-\infty}^{\infty} \{E_1^{2n}(t) + E_2^{2n}(t) + \cdots + E_n^{2n}(t)\} dt}.$$

The denominator in this expression has been chosen so as to normalize g_B^n to its background value [i.e., $g_B^n(\infty, \infty, \cdots, \infty) = 1$]. This correlation function is termed "fast" since it will contain rapidly varying phase factors $\sim\cos(\omega_j \tau_{j-1})$ in its various components.

For those experimental arrangements producing a zero background correlation, the general nth-order background-free fast correlation function is given by the expression

$$g_0^n(\tau_1, \tau_2, \cdots, \tau_{n-1}) = \frac{\int_{-\infty}^{\infty} \{E_1(t)E_2(t+\tau_1)\cdots E_n(t+\tau_{n-1})\}^2 dt}{\int_{-\infty}^{\infty} \{E_1(t)E_2(t)\cdots E_n(t)\}^2 dt} \quad (2)$$

such that $g_0^n(0, 0, \cdots, 0) = 1$. The fundamental difference

0018-9197/80/0900-0990$00.75

TABLE I
CONTRAST RATIOS $g_B^n(0, 0, \cdots, 0)$ AND $G_B^n(0, 0, \cdots, 0)$ VERSUS n

n	$CR(g_B^n)$	$CR(G_B^n)$	$CR(g_B^n)/CR(G_B^n)$
2	8:1	3:1	2.67
3	243:1	31:1	7.84
4	16,384:1	679:1	24.12
5	1,953,125:1	25,581:1	76.35

between the background-free method and that producing a background level in the measurement is reflected in the very different natures of the expressions (1) and (2). Thus, g_0^n vanishes if any of the τ_j is $\gg\tau_{pj}$, where τ_{pj} is the jth pulse duration, while g_B^n remains finite for any and all values of the τ_j.

To resolve the fast variations inherent in the correlation functions defined above requires controlling the spatial variations on a scale of roughly $\frac{1}{10}$ that of the shortest wavelength involved [7]. It is not surprising, therefore, that what is much more commonly measured in practice are the "slow" correlation functions given by the expressions

$$G_B^n(\tau_1, \tau_2, \cdots, \tau_{n-1}) = \langle g_B^n(\tau_1, \tau_2, \cdots, \tau_{n-1})\rangle_{\tau,n}$$
$$G_0^n(\tau_1, \tau_2, \cdots, \tau_{n-1}) = \langle g_0^n(\tau_1, \tau_2, \cdots, \tau_{n-1})\rangle_{\tau,n} \quad (3)$$

for the cases with and without background, respectively. The multidimensional "optical time average" denoted in (3) is defined as

$$\langle [\ ]\rangle_{\tau,n} \equiv \frac{1}{T_2 T_3 \cdots T_n} \int_{[\tau_1-(T_2/2)]}^{[\tau_1+(T_2/2)]} \int_{[\tau_2-(T_3/2)]}^{[\tau_2+(T_3/2)]} \cdots \int_{[\tau_{n-1}-(T_n/2)]}^{[\tau_{n-1}+(T_n/2)]} \cdot [\ ]\, d\tau_1\, d\tau_2 \cdots d\tau_{n-1} \quad (4)$$

with

$$\omega_j^{-1} \ll T_j \ll \tau_{pj}; \quad j = 2 \text{ to } n \quad (5)$$

where τ_{pj} is the FWHM duration of the jth pulse. Note that the slow correlation functions are determined solely by the time dependences of the pulse envelopes $\xi_j(\tau_{j-1})$; all information regarding the phase perturbations $\phi_j(\tau_{j-1})$ is lost as a consequence of the failure of the slow correlations to resolve the much faster optical frequency variations $\sim\cos(\omega_j\tau_{j-1})$.

B. nth-Order Autocorrelation Functions

In the nth-order autocorrelation, one mixes n "replicas" of a single pulse so that

$$g_B^n(\tau_1, \tau_2, \cdots, \tau_{n-1}) = \frac{\int_{-\infty}^{\infty} \{E(t) + E(t+\tau_1) + \cdots + E(t+\tau_{n-1})\}^{2n}\, dt}{n\int_{-\infty}^{\infty} E^{2n}(t)\, dt} \quad (6)$$

for the fast autocorrelation with background, while

$$g_0^n(\tau_1, \tau_2, \cdots, \tau_{n-1}) = \frac{\int_{-\infty}^{\infty} \{E(t)E(t+\tau_1)\cdots E(t+\tau_{n-1})\}^2\, dt}{\int_{-\infty}^{\infty} E^{2n}(t)\, dt} \quad (7)$$

for the fast background-free autocorrelation function. The slow nth-order autocorrelations are given by the $\langle [\ ]\rangle_{\tau,n}$ optical averages of (6) and (7) where $\langle [\ ]\rangle_{\tau,n}$ is as defined by (4).

A parameter of critical significance for autocorrelation measurements with background is the so-called "contrast ratio," defined as the ratio of the peak value of the autocorrelation function (at $\tau_i = 0$, $i = 1$ to $n-1$) to its background value. General analytic formulas are derivable for the values of the contrast ratios for nth-order fast and slow autocorrelations from (6) and (4). They are

$$CR\,(g_B^n) = g_B^n(0, 0, \cdots, 0) = n^{2n-1} \quad (8)$$

and

$$CR\,(G_B^n) = G_B^n(0, 0, \cdots 0) = n!(n-1)! \sum_{i_1=0}^{n} \sum_{i_2=0}^{i_1} \sum_{i_3=0}^{i_2} \cdots \sum_{i_{n-1}=0}^{i_{n-2}} \left[\frac{1}{(n-i_1)!(i_1-i_2)!(i_2-i_3)!\cdots(i_{n-2}-i_{n-1})!(i_{n-1})!}\right]^2. \quad (9)$$

Both contrast ratios increase rapidly with n, particularly that for the fast autocorrelation g_B^n. Table I lists the values of $CR\,(g_B^n)$ and $CR\,(G_B^n)$ and their ratio $CR\,(g_B^n)/CR\,(G_B^n)$ for $n = 2$-5. It is emphasized that these values of $CR\,(G_B^n)$ are calculated assuming a smooth, slowly varying envelope and phase perturbation for the optical pulse; different values for $CR\,(G_B^n)$ are obtained if $E(t)$ is taken to represent a pulse with substructure or a noisy "burst" of pulses, etc. [1], [8].

C. Second-Order Autocorrelation Functions and Model Pulse Shapes

The most commonly measured autocorrelation is that of a pulse with a single replica of itself, i.e., $n = 2$. For this special case

$$g_B^2(\tau) = 1 + \frac{2\int_{-\infty}^{\infty} E^3(t)E(t+\tau)\,dt + 2\int_{-\infty}^{\infty} E(t)E^3(t+\tau)\,dt + 3\int_{-\infty}^{\infty} E^2(t)E^2(t+\tau)\,dt}{\int_{-\infty}^{\infty} E^4(t)\,dt}.$$

For a slowly varying pulse envelope $\xi(t)$ and phase deviation $\phi(t)$, the τ-averaging can be performed on (10) to yield the slow autocorrelation with background as

$$G_B^2(\tau) = 1 + 2\frac{\int_{-\infty}^{\infty} \xi^2(t)\xi^2(t+\tau)\,dt}{\int_{-\infty}^{\infty} \xi^4(t)\,dt}$$

$$= 1 + 2\frac{\int_{-\infty}^{\infty} I(t)I(t+\tau)\,dt}{\int_{-\infty}^{\infty} I^2(t)\,dt} \tag{11}$$

where $I(t) = \text{cst}\ \xi(t)$ is the optical time-averaged pulse intensity.

For the background-free second-order autocorrelation

$$g_0^2(\tau) = \frac{\int_{-\infty}^{\infty} E^2(t)E^2(t+\tau)\,dt}{\int_{-\infty}^{\infty} E^4(t)\,dt} \tag{12}$$

while

$$G_0^2(\tau) = \frac{\int_{-\infty}^{\infty} \xi^2(t)\xi^2(t+\tau)\,dt}{\int_{-\infty}^{\infty} \xi^4(t)\,dt}$$

$$= \tfrac{1}{2}\,[G_B^2(\tau) - 1]. \tag{13}$$

To explicitly illustrate the differences between these various classes of autocorrelation functions, it is instructive to adopt a specific model for $E(t)$ so that the corresponding autocorrelations may be evaluated. To this end, a Gaussian pulse having a linear phase "chirp" is chosen, i.e.,

$$E(t) = \xi(t)\cos(\omega t + \phi(t)) = \xi_0 e^{-t^2/2T^2}\cos\left(\omega t + \frac{at^2}{T^2}\right). \tag{14}$$

The corresponding fast autocorrelation functions are

$$g_B^2(\tau) = 1 + 4e^{-(3+4a^2)\tau^2/8T^2}\cos(\omega\tau)\cos[a^2\tau^2/2T^2] + e^{-(1+4a^2)\tau^2/2T^2}\cos(2\omega\tau) + 2e^{-\tau^2/2T^2} \tag{15}$$

and

$$g_0^2(\tau) = \tfrac{2}{3}e^{-\tau^2/2T^2} + \tfrac{1}{3}e^{-(1+4a^2)\tau^2/2T^2}\cos(2\omega\tau) \tag{16}$$

while the time-averaged slow autocorrelation functions are

$$G_B^2(\tau) = 1 + 2e^{-\tau^2/2T^2} \tag{17}$$

$$G_0^2(\tau) = e^{-\tau^2/2T^2}. \tag{18}$$

Clearly there is a progressive simplification in going from g_B^2 through to G_0^2. This simplification, however, is gained at the cost of "loss of information" about the original pulse characteristics. Thus, information on the linear phase chirp appears only in the fast autocorrelations. Although for the simple, idealized pulse of (14), the two slow autocorrelation functions G_B^2 and G_0^2 are effectively equivalent; subtle but important differences will exist in the nature of these two functions in those cases where the pulse is structured or "noisy" [1], [8].

Table II presents a list of calculations of $G_0^2(\tau)$, bandwidth products $\Delta\nu\Delta t$, and the relationship between pulsewidth τ_p and autocorrelation width τ_G (both FWHM) for a variety of "model" pulse shapes arranged in order of decreasing τ_p/τ_G values. All parameters and formulas in Table II are exact and analytic with one exception: the expression for τ_G/τ (and hence, also that for τ_p/τ_G) for the asymmetric two-sided exponential pulse is an equation fitted to the numerically calculated values of τ_G with an $|\text{error}| \leqslant 0.3$ percent for all $0 \leqslant R \leqslant 1$. Note that this expression as well as $\Delta\nu\Delta t$ for the same pulse model are symmetric with respect to the value $R = \frac{1}{2}$.

III. The CW Autocorrelator

The CW autocorrelation interferometer is illustrated schematically in Fig. 1. The ultrathin ($\approx 7\ \mu$) pellicle M divides the incoming laser pulse into two equal intensity pulses. One of these pulses travels to and is retroreflected (parallel within 2 arcsec) by a small, antireflection coated, corner cube prism attached to and coaxial with the speaker cone. The other pulse is reflected back, spatially displaced by ≈ 10 mm, by a small stationary rooftop prism. These two returning pulses are then reflected and transmitted, respectively, by the pellicle onto a simple biconvex lens L (focal length = 50 mm), which focuses the two beams into a 100 μm thick KDP crystal cut to produce type I SHG for 600 nm light at approximately normal incidence. The SH UV light emerges from the crystal along the bisection of the diverging fundamental beams and so the combination of a UV transmitting/visible absorbing filter (Corning 7-54) followed by an aperture ensures that only the SHG light enters the photomultiplier tube (RCA 1P28). To enable calibration of the autocorrelator, the rooftop prism was mounted on a 50 mm travel precision translation stage.

The 7 in diameter audio speaker (Philips AD7066/W8) was driven through a 75 Ω series resistor by an amplified signal from a sine wave generator at a frequency $f = 30$ Hz. The maximum stroke obtainable with this particular speaker was 9 mm (peak-to-peak travel) corresponding to a (measured)

TABLE II
SECOND-ORDER AUTOCORRELATION FUNCTIONS AND BANDWIDTH PRODUCTS FOR VARIOUS PULSESHAPE MODELS

$I(t)$ $(x \equiv t/T)$	$\Delta\nu\Delta t$	τ_p/T	$G_0^2(\tau)$ $(y \equiv \tau/T)$	τ_G/T	τ_p/τ_G
1. Square $I(t) = \begin{cases} 1; & \lvert t\rvert \le T/2 \\ 0; & \lvert t\rvert > T/2 \end{cases}$	0.8859	1	$\begin{cases} 1-\lvert y\rvert; & \lvert\tau\rvert \le T \\ 0 & ; \lvert\tau\rvert > T \end{cases}$	1	1
2. Parabolic $I(t) = \begin{cases} 1-x^2; & \lvert t\rvert \le T \\ 0 & ; \lvert t\rvert > T \end{cases}$	0.7276	$\sqrt{2}$	$\begin{cases} 1-\frac{5}{4}y^2+\frac{5}{8}\lvert y\rvert^3-\frac{1}{32}\lvert y\rvert^5; & \lvert\tau\rvert \le 2T \\ 0 & ; \lvert\tau\rvert > 2T \end{cases}$	1.6226	0.8716
3. Diffraction function $I(t) = \frac{\sin^2 x}{x^2}$	0.8859	2.7831	$\frac{3}{2y^2}\left[1-\frac{\sin 2y}{2y}\right]$	3.7055	0.7511
4. Gaussian $I(t) = e^{-x^2}$	0.4413	$2\sqrt{\ln 2}$	$e^{-y^2/2}$	$2\sqrt{2\ln 2}$	0.7071
5. Triangular $I(t) = \begin{cases} 1-\lvert x\rvert; & \lvert t\rvert \le T \\ 0 & ; \lvert t\rvert > T \end{cases}$	0.5401	1	$\begin{cases} 1-\frac{3}{2}y^2+\frac{3}{4}\lvert y\rvert^3 & ; \lvert\tau\rvert \le T \\ 2-3\lvert y\rvert+\frac{3}{2}y^2-\frac{1}{4}\lvert y\rvert^3; & T < \lvert\tau\rvert \le 2T \\ 0 & ; \lvert\tau\rvert > 2T \end{cases}$	1.445	0.6922
6. Hyperbolic sech $I(t) = \operatorname{sech}^2 x$	0.3148	1.7627	$\frac{3}{\sinh^2 y}\left[y\coth y - 1\right]$	2.7196	0.6482
7. Lorentzian $I(t) = \frac{1}{1+x^2}$	0.2206	2	$\frac{1}{1+(y/2)^2}$	4	0.5000
8. One-sided exp $I(t) = \begin{cases} e^{-x}; & t \ge 0 \\ 0 & ; t < 0 \end{cases}$	0.1103	$\ln 2$	$e^{-\lvert y\rvert}$	$2\ln 2$	0.5000
9. Symmetric two-sided exp $I(t) = e^{-2\lvert x\rvert}$	0.1420	$\ln 2$	$(1+2\lvert y\rvert)e^{-2\lvert y\rvert}$	1.6783	0.4130
10. Asymmetric two-sided exp $I(t) = \begin{cases} e^{t/T_1}; & t < 0 \\ e^{-t/T_2}; & t \ge 0 \end{cases}$ with $T = T_1 + T_2$, $R = T_1/T$: $0 \le R \le 1$	$\frac{\ln 2}{2\pi}\left[\frac{-b+\sqrt{b^2+4a}}{2a}\right]^{1/2}$ with $a = R^2(1-R)^2$, $b = R^2+(1-R)^2$	$\ln 2$	$\frac{T_2}{T_2-T_1}e^{-\lvert\tau\rvert/T_2} - \frac{T_1}{T_2-T_1}e^{-\lvert\tau\rvert/T_1}$	$2\ln 2 + 0.6857R(1-R) + 1.9300R^2(1-R)^2$	$\frac{\ln 2}{[2\ln 2 + 0.6857R(1-R) + 1.9300R^2(1-R)^2]}$

maximum dynamic range of 60 ps. It was found that, in general, there existed an appreciable phase difference between the signal applied to the speaker and its actual response, i.e., cone displacement. This phase shift varied markedly with the frequency f of the applied signal and, to a much lesser extent, with signal strength. Since it is essential that the signal driving the x-axis of the oscilloscope display be directly proportional to $|\tau|$, i.e., the speaker displacement, in order to obtain a linear display of $G_0^2(\tau)$, the signal applied to the oscilloscope was derived from a variable phase shift oscillator circuit which was fed by a portion of the signal from the sine wave generator. This circuit was used to accurately adjust the phase shift of the sine wave driving the oscilloscope so as to produce a phase difference between it and the speaker motion of either exactly 0 or π. The correct phase shift is easily recognized by the fact that it produces a display of $G_0^2(\tau)$ which is centered about "$x = 0$" on the oscilloscope and which is maximum (i.e., $G_0^2(\tau = 0)$ when the speaker cone is motionless.

Although in theory the autocorrelation traces produced as the speaker travels first outward and then inward should overlap identically, it was found in practice that the overlap was never exact even with "fine" adjustments to the speaker cone motion. To circumvent this problem, a second square-wave (±10 V) signal was derived from this phase shift oscillator circuit which was exactly in-phase with the phase shifted sine wave used to drive the x-axis of the display. This square-wave was applied to the z-axis of the oscilloscope and thus blanked those signals corresponding to one particular direction of travel of the speaker.

Typical autocorrelation traces of 600 nm picosecond pulses

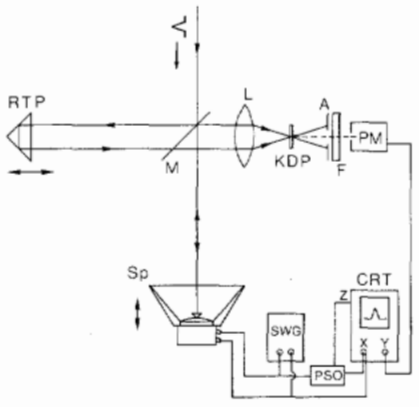

Fig. 1. CW autocorrelator schematic: rooftop prism (RTP); mirror beamsplitter (M); filter (F); photomultiplier (PM); speaker with corner cube prism (SP); sine wave generators (SWG); phase shift oscillator (PSO).

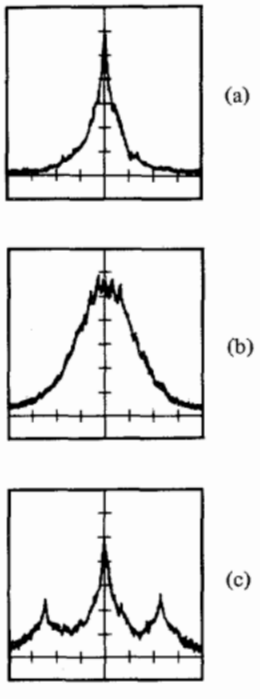

Fig. 2. Autocorrelation traces of picosecond pulses from CW synchronously mode-locked Rh 6G dye laser: (a) without fine tuning etalon; (b) with fine tuning etalon ($\Delta\nu = 40$ GHz); (c) without etalon and using a 200 μm thick plane parallel plate to sample beam.

from a CW synchronously mode-locked (CWSML) Rh 6G dye laser pumped by an acoustooptically mode-locked Ar ion laser are shown in Fig. 2. Fig. 2(a) shows the output from the laser when only a broad tuning wedge ($\Delta\nu \approx 200$ GHz) is employed in the cavity. The shape of $G_0^2(\tau)$ in this case is approximately (see Fig. 5) $\exp(-|\tau|/T)$ which corresponds to a single sided exponential pulse τ_p of $\simeq 0.8$ ps. The autocorrelation trace shown in Fig. 2(b) corresponds to the pulses produced when a fine tuning etalon ($\Delta\nu = 40$ GHz) is also employed in the dye cavity in addition to the broad tuning wedge. The shape of $G_0^2(\tau)$ in this case corresponds almost perfectly to that produced by sech^2 laser pulses (Table II) of a bandwidth limited

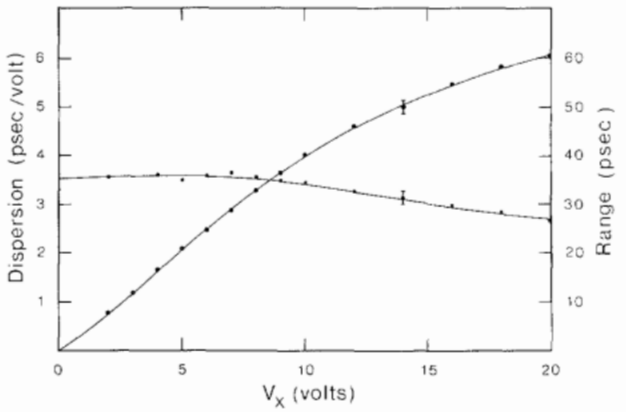

Fig. 3. Dispersion and dynamic range of the autocorrelator versus drive signal strength (α V_x).

duration of 8 ps. The traces in Fig. 2 were photographed with a shutter speed of $\frac{1}{60}$ s, and so are single-sweep traces of $G_0^2(\tau)$. In practice, autocorrelation traces with good signal-to-noise characteristics were obtained when using only $\approx$10 percent of the CW dye laser output (typical output $\approx$1 kW peak) thus enabling the use of the autocorrelator as a permanent, on-line pulsewidth monitor. This is the case for Fig. 2(c) which shows the autocorrelation observed when a thin, uncoated beam splitter at 45° is used to divert $\approx$8 percent of the dye laser output [pulses as in Fig. 2(a)] into the autocorrelator. The secondary peaks in the trace in Fig. 2(c) are 24 ps apart corresponding exactly to the beam-splitter thickness of 1.30 mm and so provide a convenient, accurate, and permanent calibration of the trace. This ability of the CW autocorrelator to work with only a small sample of the laser beam is a most useful characteristic of the device since it enables one to easily monitor pulsewidth behavior at any point in the laser system (e.g., before, within, and after a series of dye amplifier stages in the present system) by simply diverting a sample of the beam back to the autocorrelator.

It is desirable to use the autocorrelator over a large range of "temporal amplification," i.e., from a small speaker stroke to maximum speaker stroke for a fixed "X-axis display length" on the oscilloscope. Ideally, the "dispersion" of the autocorrelator measured in ps/V (here "volt" represent signal strength of the X-axis display which is linearly related to the volts applied to the speaker) should be a constant, while the total range of the sweep (peak-to-peak) should increase exactly linearly with voltage. Measurements of these two parameters were made for the 7 in speaker and the results are shown in Fig. 3. The abscissa is the x-axis voltage with 20 V corresponding to maximum speaker displacement (9 mm peak-to-peak). As the data show, the linearity of the speaker is excellent over most of the range and shows a slight leveling off only as the maximum stroke is approached (in this limit, the voice coil begins oscillating beyond the field of the permanent magnet during parts of the cycle and thus increasing signal strength produces proportionally lessened cone displacement). The dispersion (ps/V) is effectively constant from 0 to $\frac{2}{3}$ maximum speaker displacement (range 0–40 ps). As well, constancy of the dispersion with respect to x for a fixed signal

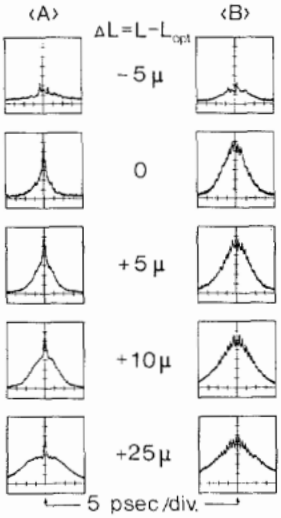

Fig. 4. Variation of pulsewidth with dye cavity length (a) with and (b) without fine tuning etalon.

strength was checked for a number of different voltages and it was found that the dispersion versus position on the x-axis display was constant to better than ±15 percent over its total range and constant to within ±10 percent over the central $\frac{2}{3}$ of the dislay for any given driving signal strength.

As a means of studying both the behavior of the dye laser and the ability of the CW autocorrelator to provide "on-line" monitoring of that behavior, the variation of the picosecond pulsewidths with changes in the length of the dye laser cavity was examined in detail. Due to the very nature of the CW synchronous mode-locking technique, well-defined picosecond pulses are produced only if the dye laser cavity length is matched to and stable to within a few microns of the argon ion pump laser cavity length (or, more generally, any simple multiple or submultiple of it). The dye cavity length was varied by a motorized precision translation unit in steps of 1 μm (Ealing translation stage 34-2419) and the results of the CW autocorrelator measurements are shown in Fig. 4 both for the cases of the cavity with [Fig. 4(a)] and without [Fig. 4(b)] the fine tuning etalon. As these figures dramatically show, the setting of the dye laser length is critical, particularly in the direction of a shortened cavity, with a shortening by as little as 5 μm producing virtually complete disintegration of the dye laser output. The effect on the pulse of lengthening the dye cavity is not so drastic, although the departure from optimum pulse shape (at $\Delta L = 0$) is, in reality, just as rapid. Thus, particularly as Fig. 4(a) shows, a length increase of $\geqslant 5$ μm produces what is clearly a "broadened" pulse with picosecond substructure. For the sake of comparison, Fig. 5 shows the conventional autocorrelation traces obtained on a strip chart recorder with the speaker stationary and the roof top prism slowly translated (scan time ~1 min). Fig. 5(a) and (b) correspond to their counterparts in Fig. 4(a) with $\Delta L = 0$ and +10 μ, respectively. The points in Fig. 5(a) are an exp $(-|\tau|/T)$ fit to the autocorrelation trace which corresponds to a single-sided exponential laser pulse with $\tau_p \sim 0.8$ ps. More generally, however, slightly better fits are obtained by using the function

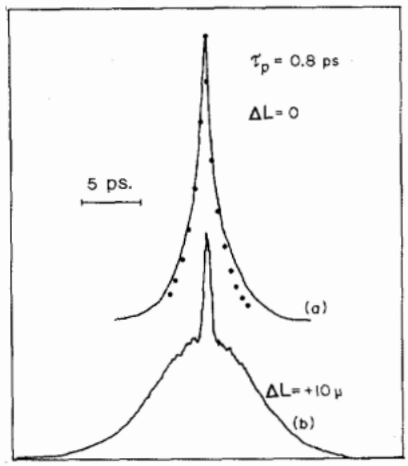

Fig. 5. Conventional recording of the autocorrelation traces for (a) $\Delta L = 0$ and (b) $\Delta L = +10$ μ.

corresponding to an asymmetric two-sided exponential pulse with $R \approx 0.1$ (see Table II).

IV. Conclusion

CW correlation techniques will play an increasingly important role in the measurement and analysis of picosecond and subpicosecond laser pulses and dynamical events. A simple, inexpensive but yet precise CW picosecond autocorrelator has been described and typical results of picosecond pulsewidth measurements from a CW synchronously mode-locked Rh 6G laser presented. Moreover, the results on the criticality of the dye laser cavity length serve to underline the advantage of the CW autocorrelator in quickly and accurately permitting optimization of the dye laser output with respect to this and other critical parameters. Considerable practical advantage would be gained by the extension of this technique to a dynamic range $\gg$60 ps, and we are currently making progress in this direction.

Acknowledgment

It is a pleasure to acknowledge the expert assistance and advice given by W. Panning on speaker characteristics and the detailed design of the phase shift oscillator circuitry.

References

[1] Detailed reviews of ultrashort pulse measurements and techniques with comprehensive referencing are given by E. P. Ippen and C. V. Shank, "Techniques for measurements," in *Ultrashort Light Pulses*, S. L. Shapiro, Ed. New York: Springer-Verlag, 1977, pp. 83–122; D. J. Bradley and G. H. C. New, "Ultrashort pulse measurements," *Proc. IEEE*, vol. 62, pp. 313–345, 1974.

[2] M.Maier, W. Kaiser, and J. A. Giordmaine, "Intense light bursts in the stimulated Raman effect," *Phys. Rev. Lett.*, vol. 17, pp. 1275–1277, 1966.

[3] J. A. Armstrong, "Measurement of picosecond laser pulse widths," *Appl. Phys. Lett.*, vol. 10, pp. 16–18, 1967.

[4] J. A. Giordmaine, P. M. Rentzepis, S. L. Shapiro, and K. W. Wecht, "Two-photon excitation of fluorescence by picosecond light pulses," *Appl. Phys. Lett.*, vol. 11, pp. 216–218, 1967.

[5] A. Dienes, E. P. Ippen, and C. V. Shank, "A mode-locked CW dye laser," *Appl. Phys. Lett.*, vol. 19, pp. 258–260, 1971; "Passive mode-locking of the CW dye laser," *Appl. Phys. Lett.*, vol. 21, pp. 348–350, 1972

[6] R. L. Fork and F. A. Beisser, "Real-time intensity autocorrelation interferometer," *Appl. Opt.*, vol. 17, pp. 3534–3535, 1978.
[7] J. C. Diels, E. W. Van Stryland, and D. Gold, "Investigation of the parameters affecting subpicosecond pulse durations in passively mode-locked dye lasers," in *Picosecond Phenomena*, C. V. Shank, E. P. Ippen, and S. L. Shapiro, Eds. New York: Springer-Verlag, 1978, pp. 117–120.
[8] See, e.g., M. A. Duguay, J. W. Hansen, and S. L. Shapiro, "Study of the Nd: Glass laser radiation," *IEEE J. Quantum Electron.*, vol. QE-6, pp. 725–743, Nov. 1970, and references therein.

Kenneth L. Sala was born in Winnipeg, Canada, on January 17, 1949. He received the B.Sc. degree from the University of Manitoba, Winnipeg, Canada, in 1971, the M.Eng. degree from Carlton University, Ottawa, Ont., Canada, in 1973, and the Ph.D. degree in physics from the University of Waterloo, Waterloo, Ont., Canada, in 1976.

During 1971–1976, he conducted his graduate research as a full-time guest worker with the Laser and Plasma Physics Group of the National Research Council of Canada, Ottawa, Ont. During the years 1977–1978 he was a NATO Post-Doctoral Fellow working in the Laser Physics Group, Imperial College, London, and since November 1978, he has been a Research Associate with the Picosecond Laser Spectroscopy Group in the Department of Chemistry at the University of Toronto, Toronto, Ont., Canada. His principal research interests include the production and applications of picosecond laser pulses, nonlinear optics, laser produced plasma physics, picosecond photography, and ultrafast spectroscopic processes.

Dr. Sala is a member of the American Physical Society.

Geraldine A. Kenney-Wallace was born in London, England, on March 29, 1943. She received the M.Sc. and Ph.D. degrees in chemical physics from the University of British Columbia, in 1968 and 1970, respectively.

Following post-doctoral studies at UBC and at the Radiation Laboratory, University of Notre Dame, she joined the Chemistry Faculty, Yale University, New Haven, CT, in 1972. She moved to the University of Toronto, Toronto, Ont., Canada, in 1974 and set up the Picosecond Laser Spectroscopy Group in chemistry. She is now Professor of Chemistry and a Killam Senior Research Fellow (1979–1981). Her major research interests focus on the fundamental aspects of laser-induced picosecond phenomena, including molecular dynamics, energy and electron transfer in liquids, and nonlinear optical phenomena, all of which also include important device applications in laser spectroscopy.

Prof. Kenney-Wallace is a member of the American Physical Society, the Optical Society of America, Sigma Xi, and is on the Executive Committee of the Inter-American Photochemical Society.

Gregory E. Hall was born in Geneva, NY, in 1952. He received the B.Sc. degree in chemistry from Cornell University, Ithaca, NY, in 1974, and the M.Sc. and Ph.D. degrees from the University of Toronto, Toronto, Ont., Canada, in 1976 and 1980, respectively.

His graduate research at the University of Toronto was on the laser-induced, two-photon photoionization mechanisms of organic molecules and related topics on electron localization and applications to solar energy. In July 1980 he was appointed as a Research Associate and Manager of the Laser Spectroscopy Facility, Department of Chemistry at Cornell University.

Dr. Hall is a member of the American Physical Society.